International Journal of Basic and Applied Sciences, 14 (4) (2025) 84-97

International Journal of Basic and Applied Sciences

Website: www.sciencepubco.com/index.php/IJBAS
https://doi.org/10.14419/fwa09g88
Research paper

Simulation-Based Study of Self-Excited SRG by Using Nonlinear Models and Open-Loop Excitation Strategies

V. Balasubramanian [1] *, S. Radhika [2], V. Senthil Nayagam [3]

[1] Department of Electrical and Electronics Engineering, Sathyabama Institute of Science and Technology, Chennai, India.
[2] Department of Electronics and Communication Engineering, Chennai Institute of Technology, Chennai
[3] Department of Electrical and Electronics Engineering, Sathyabama Institute of Science and Technology, Chennai, India
**Corresponding author E-mail: balaplcautomation@gmail.com*

Received: June 17, 2025, Accepted: July 27, 2025, Published: August 5, 2025

Abstract

This research offers a comprehensive examination of the operational principles and dynamic characteristics of the Switched Reluctance Generator (SRG) when functioning in self-excited mode. The focus is on the rotor's inherent inclination to align with the path of least reluctance, requiring the separate activation of each phase via appropriate power electronic converters and control systems. Recent studies emphasize the increasing importance of the SRG in renewable energy and automotive industries. The study highlights the shortcomings of linear modeling for precise simulation, especially when neglecting magnetic saturation and nonlinearities in the machine. A nonlinear model that includes magnetic saturation and utilizes a Fourier series-based inductance profile was developed in MATLAB/Simulink using data from an existing prototype. The excitation approach used a parallel capacitor alongside a half-bridge converter, and simulations were performed in open-loop mode. The research examined differences in speed, actuation angles, and load conditions, uncovering their effects on both transient and steady-state voltage performance. Results indicate that angle modulation greatly influences ignition timing and overall system efficiency. This study enhances the basic comprehension of SRG functioning under self-excited conditions and aids future uses in energy-efficient systems.

Keywords: *Self-Excited SRG; Nonlinear Models; Open-Loop Excitation Strategies; Nonlinear Model.*

1. Introduction

Electrical machines are essential tools for maintaining our contemporary way of life. They are present in many processes in the food, textile, and metallurgical industries, among others. Among them are Variable Reluctance Machines (VRMs).
Existing since the early days of research and development of electric motors and generators, they have received more attention from the scientific community due to advances in control systems and power electronics. Their operation has been the focus of work and research in the area of electrical machines.
VRMs are salient pole machines, located in both the stator and the rotor. Their operating principle is based on the tendency of the rotor to move to a position where the reluctance is minimum in the stator, which means that the inductance in the stator coil is maximum. Due to the need to know the rotor position, sensors are used to monitor the rotor position and fast switching, in order to maintain the excitation of each pole at the appropriate time, thus obtaining the benefit of the applied torque.
Its representation by mathematical models, considering the non-linear characteristics of the magnetic circuit, is necessary to carry out simulations and the closest representation of the machine to the real one for the development of control methods.
For example, in [8], a prototype was developed, supported by simulations, of a VRM with the capacity to operate as a motor for a speed range between 2,500 and 8,000 rpm. The work proved the results experimentally; the prototype should also act as a generator for a speed range between 19,200 and 32,000 rpm. In this second test, the experimental data have not yet been collected, due to the need for changes in the experimental bench, so only the simulation estimates are available.
In [29], simulating a strategy for the operation of a VRM generating AC instead of DC, it was found that it was impossible to connect it to the grid due to the harmonic effect indicated in the simulation. In [1 – 3], [5] simulations are performed and compared with real experiments, proving the efficiency of models and their applicability.
In [9], the behavior of a prototype for low-speed wind generation was verified via simulation, comparing different control and excitation strategies. In [15], the behavior of a VRM operating as a motor was analyzed for different types of power supply. In [17], a new converter model was compared with conventional ones via simulation.

2. Literature review

Touati et al. (2022) [9] aimed at enhancing the steady-state efficiency of SRGs using voltage regulation. The research offered experimental confirmation for the suggested approach, emphasizing the efficiency of sophisticated control methods in stabilizing the generator's output voltage. Their findings highlight the significance of accurate voltage control mechanisms in maintaining system reliability across different load conditions.
Li et al. (2020) [10] examined the generation traits of a double stator SRG with deflection type. Their study makes a notable contribution to structural innovation in SRGs, offering a design that boosts electromagnetic performance and increases power density. The research provided comprehensive modeling and simulation analyses, illustrating the impact of mechanical design on electrical performance.
Chirapo et al. (2020) [11] introduced a P+RES controller for the direct management of power in SRGs. Their approach combined power control with energy management tactics, demonstrating that sophisticated control algorithms can improve dynamic performance and efficiency. Simulation outcomes validated the ability of the P+RES controller to manage output power efficiently.
Sarr et al. (2020) [12] confirmed the functioning of SRGs in low-voltage DC microgrids. Their experimental research demonstrated how SRGs can be successfully incorporated into microgrid configurations, aiding in decentralized energy production. The document highlighted the dependability and flexibility of SRGs in practical low-voltage situations.
Zan et al. (2019) [13] proposed an innovative control approach built on adjusted PT control. The innovation is found in adjusting phase timing to enhance energy conversion. Simulation and experimental findings showed a notable increase in output power and a decrease in torque ripple, confirming the efficacy of the revised PT control strategy.
dos Santos Barros et al. (2017) [14] conducted extensive research on SRGs within wind generation systems. The suggested method handled significant fluctuations in wind speed, providing steady output via adaptive control. Their efforts are essential for grasping SRG efficiency in variable renewable energy sources.
Lu et al. (2021) [15] explored a microgrid configuration featuring wind-driven SRGs combined with a plug-in energy assistance system. The integration promotes energy equilibrium and grid reliability, demonstrating that SRGs can significantly aid smart grid initiatives. The system's ability to withstand different load and generation conditions was confirmed through experiments.
Araujo et al. (2021) [16] improved the efficiency of SRGs by utilizing an optimized control strategy along with a tracking method. Their approach refined the excitation profile to minimize losses and enhance overall efficiency. The research offered an effective structure for improving SRG performance via smart control.

3. Simulation platform

Computer simulations are extremely useful in improving projects and reducing implementation costs. In addition, simulations allow for tests that are difficult to implement in practice.
There are numerous applications for simulations; to perform them, a computational platform capable of this execution is necessary. In this section, the simulation platform will be presented, using the MATLAB software, in the Simulink tool with the SymPowerSystem package, which is commonly used in simulations related to dynamics.

3.1. Data preprocessing

Figure 1 shows the block diagram of the generation process proposed in the work.

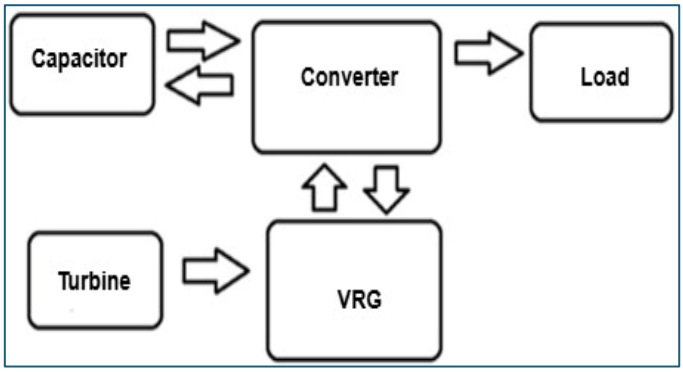

Fig. 1: Diagram of the Process to Be Simulated.

Observing Figure 1, the central pillar in the process will be the converter, which is how the interaction of the Variable Reluctance Generator (VRG) with the capacitor and the load occurs. Because the converter plays a fundamental role in the process, it is important to choose an efficient type. There are publications looking for new drive topologies and converters such as [12], [13], [17], [25], [31]. For this work, the half bridge converter (HB) was chosen because it is commonly used and easy to adapt to operation in self-excited mode.
The capacitor block refers to the excitation of the machine. The focus of this work is the activation of the VRG in self-excited mode, in which the excitation of the phases was performed by inserting a capacitor in parallel to the arms of the converter. Through the converter, the capacitor discharges and charges with each excitation cycle of the generator.
The turbine block refers to the torque (or torque), which is the source of mechanical force on the machine shaft, which can be wind, hydraulic, or another possible mechanical energy source. Usually, for experimental purposes, a motor is used, coupled to the VRM shaft, which makes it easier to control speed and torque.
The load can be chosen to simulate different applications. In this work, the generator operates in isolation; for this purpose, resistive loads were placed on its terminals.
The VRG block refers to the dynamic behavior of the VRM operating as a generator and will be implemented in the simulation using the mathematical model developed in the previous section.

3.2. Proposed static converter

Among the available topologies, the Half Bridge (HB) converter was used for the simulation, which is shown in Figure 2.

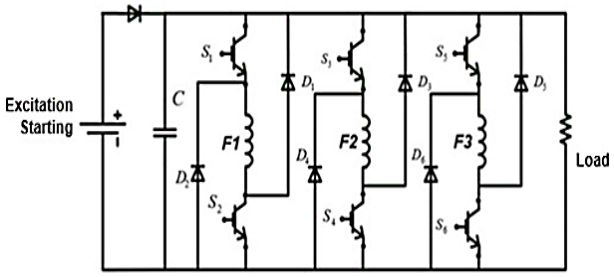

Fig. 2: HB Converter.

The excitation source is used to start the generator. After the start of operation, the capacitor C is charged and starts to provide excitation to the machine. In a rural environment, for example, a battery can be used to perform the function of the excitation source. The inductances F1, F2, and F3 represent the phase windings of the VRG, and the resistive load is inserted to check the system's performance. Each arm of the converter consists of a pair of switches and a pair of diodes; therefore, for a three-phase machine, the converter has three arms.

3.3. Machine under investigation

The pre-existing prototype, on which the simulations of this work are based, is a 6x4 VRM designed and tested by Borges [1], [36], a machine that was the subject of other studies [1 - 3]. Figure 3 shows a photo of the constructed prototype.

Fig. 3: Machine Under Study.

Photo taken from the 6x4 VRM, which is the subject of this work. The VRG windings have 50 turns per pole, totaling 100 turns per phase, and support a current of approximately 10 A [1]. The main characteristics of the prototype are shown in Figure 4. The SRG is a 1 HP, 1200 rpm machine designed for efficient performance in dynamic applications like EVs and renewables. It features a 30° conduction angle, low viscous friction (0.026 N·m·s), and compact dimensions with a 140 mm stator and 70 mm rotor. A 107 mm stack length and 12 mm yoke prevent saturation. With 100 turns per phase, 220 V, and 10 A rating, it ensures strong magnetic performance and compatibility with low-voltage systems. A low moment of inertia (0.0028 kg·m²) enables quick response to load changes, making it ideal for transient conditions.

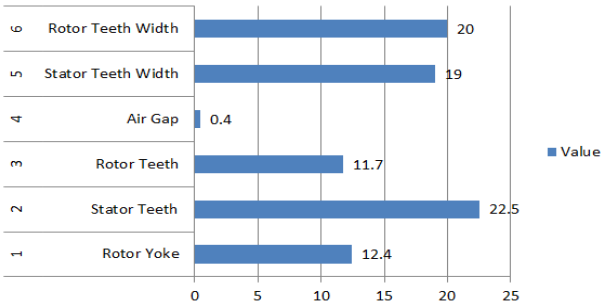

Fig. 4: The Main Characteristics of the Prototype.

Figure 4 contains the characteristics of the prototype on which the simulations performed in this work are based.
The data in Figure 4 are present in [1 - 3]; several of these characteristics are used as inputs for performing the simulation.

3.4. Computational platform

Developed in MATLAB software, more specifically in the SIMULINK platform with the SIMPOWERSYSTEM component bank, Figure 5 is the root of the computational platform. The block in the center includes the subsystems that make up the simulation; on the left are the inputs: mechanical torque (torque), the terminals of the mesh containing the capacitor and the initial excitation source; on the right are the outputs connected to the load terminals.

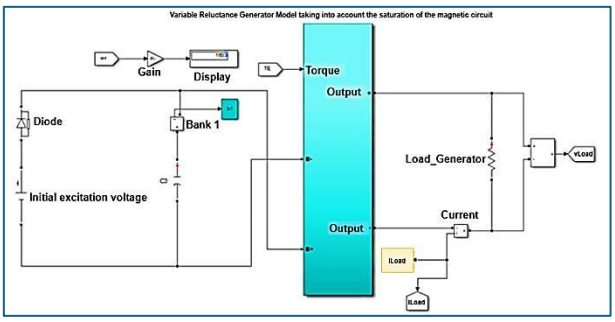

Fig. 5: Simplified Central Block of the Simulation.

The central block of the platform includes the subsystems. On the left is the initial excitation source in series with a diode, which is set in parallel with the capacitor. This source is responsible for performing the first excitation and initially charging the capacitor in order to start the generator operation. The excitation source is continuous, usually with a voltage equivalent to 5% to 10% of the voltage generated in steady state by the generator [2], [3]. After generation begins, the voltage at the load terminals becomes greater than the voltage of the initial excitation source; thus, the diode is reverse polarized and the source ends its influence on the system. The upper input on the left receives the torque applied to the machine shaft.
In this work, constant speeds will be used: 800, 1200, 1600, and 2000 rpm. Thus, the mechanical torque applied can vary according to the load.
The two lower inputs on the left are for excitation. On the right are the system voltage outputs on the resistive load.
The block in the center condenses the converter and VRG subsystems. Starting with the converter subsystem seen in Figure 6:

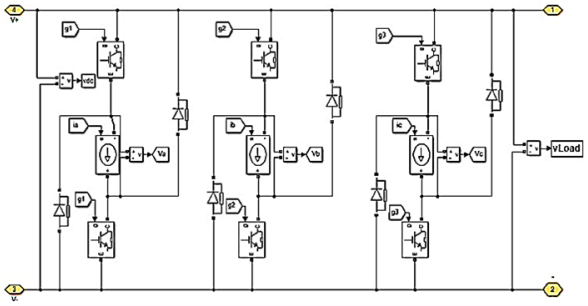

Fig. 6: HB Converter Subsystem.

The HB converter is represented using the SIMPOWERSYSTEM library. Each arm of the converter is composed of two IGTB switches and two diodes. The control of the trigger angles of the switches is performed in open loop; the angles of the tests performed in [1] were used, phase A (85.3° to 25.3°), phase B (55.3° to 85.3°), and phase C (25.3° to 55.3°).
The variables “V+” and “V-” refer to the inputs “E+” and “E-”, which are connected to the excitation source, while “1” and “2” refer to “Output+” and “Output-” connected to the load. The controlled current sources located in the middle of the arms represent the current flowing through the machine windings (Ia, Ib, and Ic). The currents are the output variables of the state matrix and are calculated in the next subsystem, which can be seen in Figure 7. The controlled sources allow the calculated currents to be reproduced in the position occupied by the machine windings, inside the converter arm.

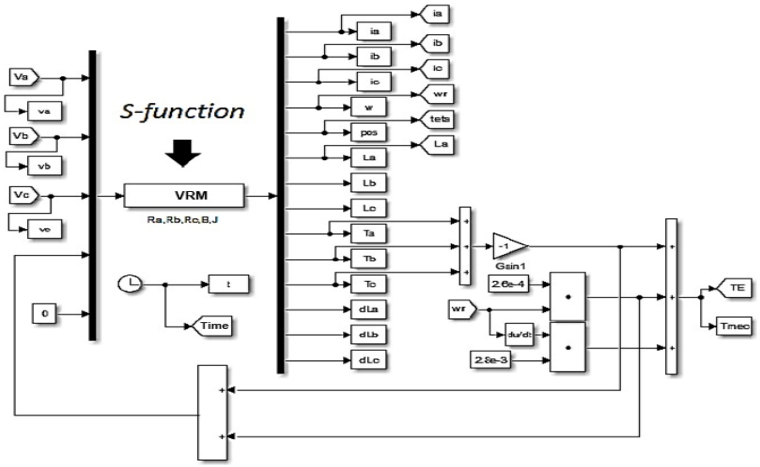

Fig. 7: VRM Behavioral Subsystem.

This subsystem simulates the Variable Reluctance Machine (VRM) behavior operating as a generator. To do this, the S-function is used, which solves the machine's state equations using numerical integration through MATLAB functions. The solution is iteratively performed in the time domain; thus, the variables feed back into the simulation at each cycle.

The inputs and outputs of this subsystem are those of the state matrix as seen in equation 3.56, inputs: phase voltages, inductance profile, VRM construction characteristics, and torque; outputs: phase currents, phase inductance, electromagnetic and mechanical torque, rotor speed, and position.
The winding resistance, moment of inertia, and viscous friction data refer to the machine's construction aspects, shown in Figure 4 and inserted into the routine.
The output currents of this subsystem are the inputs to the controlled current sources of the converter subsystem (figure 6), while the phase voltages collected in the converter feed back to its input. The electromagnetic torque and viscous friction losses add up and feed back to the system as mechanical torque; the speed is kept constant.
The S-function considers the incremental inductance profile deduced in the previous section; therefore, it takes into account magnetic saturation.

3.5. Preliminary results

Using the equations of state deduced in the previous section, the incremental inductance profile and the data in Figure 4 regarding the machine's construction parameters, together with the computational model, dynamic simulations of the VRG 6x4 operating in self-excited mode can be performed.
The first simulation was performed for a fixed shaft speed of 1600 rpm, the initial excitation source with a voltage of 20 V and the generator load resistance of 40 Ω; the time step was 3e-06. Figure 8 shows the load voltage during the transient and the beginning of the steady state, where the maximum voltage value was 101.2 V.

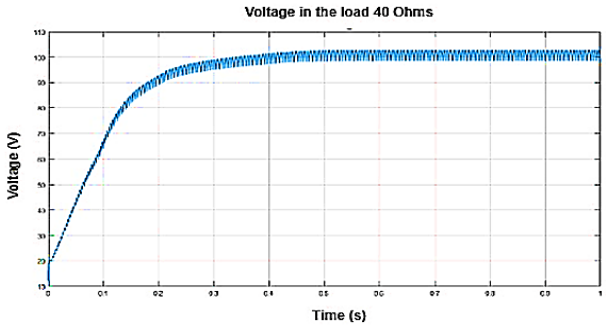

Fig. 8: Load Voltage.

The curve begins with the excitation source injecting the first charge into the capacitor. Then, the charge and discharge cycle causes an increase in the generated current until the system reaches the steady state. This transient is called igniting. Figure 9 illustrates the current increases in each phase and the load during the transient state. The peak phase current was 24.2 A, and the load current was 2.6 A.
During ignition, the current increases lead to an increase in the flux linkage. This incremental cycle continues until the magnetic saturation of the material occurs. Figure 10 depicts the inductance, phase current, and firing angle in the transient and steady state. It is possible to observe the increase in current during the transient; after the end of the trigger signal, the current continues to increase for a short period, which does not occur during the steady state due to saturation.

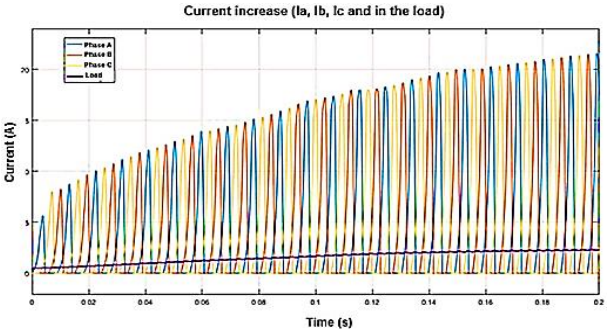

Fig. 9: Phase Current Increases.

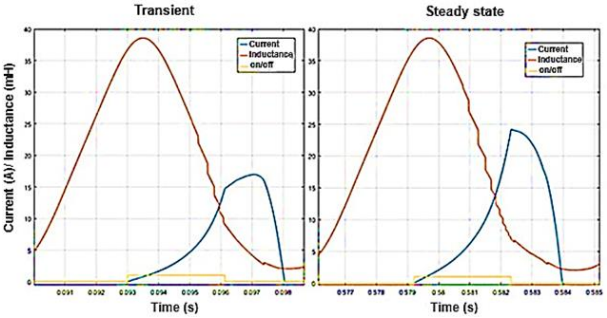

Fig. 10: Phase Inductance and Current.

The visible variation in the inductance profile with the increase in current occurs because this is the incremental inductance, which is fed back by the current, so that this effect is more pronounced during the steady state, when it reaches saturation of the magnetic circuit.

The simulation of the self-excited VRG depends on this characteristic. If neglected, the current and flux would increase in an infinitely positive feedback loop, resulting in values that do not match reality. For comparison purposes, the same computational platform was used with the same parameters as the previous simulation. However, the S-function subsystem used a model that disregards magnetic saturation. Figure 11 shows the load voltage.

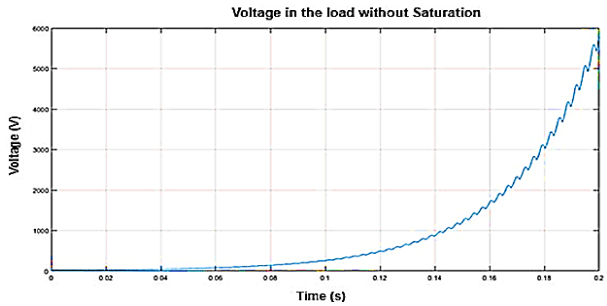

Fig. 11: Voltage at A 40 Ω Load, Disregarding Saturation.

Disregarding magnetic saturation, the load voltage reaches absurd values during the simulation, exceeding the 5000 V level during ignition, before 0.2 s of simulation. Figure 12 shows the load voltage for the models with and without saturation.

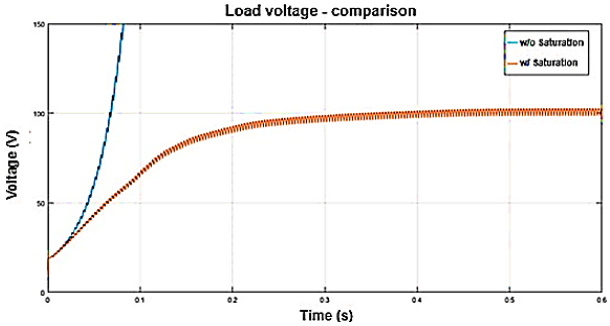

Fig. 12: Comparison between Models.

Load voltage (40 Ω) for the model that disregards saturation in blue and the one that does consider it in red.
This comparison shows the impossibility of simulating the VRG in self-excited mode, using a linear inductance profile, disregarding magnetic saturation.
In this section, the computational model to be used for the dynamic simulations of the Variable Reluctance Generator, in self-excited mode with a parallel capacitor, was presented. The platform was built using MATLAB software, in the SIMULINK environment with the SIMPOWERSYSTEM library.
The Converter chosen for the platform was the HB, and the equations deduced in the previous section were implemented in the subsystem involving the s-function. The machine construction parameters required for the simulation are based on a real VRG, presented in Figure 4.
The platform allowed the first simulation presented in this section. A model disregarding magnetic saturation was simulated using the same platform, proving the impossibility of simulating the VRG in self-excited mode in this way.
The data collected from this simulation could be used to design an experimental bench; the choice of converter components and loads can be deduced considering a safety margin; the use of simulation in projects is used in many works such as [1,2,3].
In the next section, the platform will be used to perform analyses of the VRG behavior with changes in the speed applied to the shaft and in the drive angles.

4. Speed variation and on/off angles

The simulation platform presented in the previous section allows the dynamic simulation of the VRG 6x4 operating in self-excited mode in open loop. Assuming an application in an isolated environment, such as a rural environment. Analyses of the machine's behavior for isolated application, with changes in its firing angles, and with variable speeds and loads were performed.
The ignition has an incremental effect at each cycle; a better analysis of this period is interesting and will be carried out in this section.
VRMs used for automotive or aerospace applications usually work at speeds above the machine's nominal speed, while machines operating in wind farms use lower speeds with higher torque on the shaft [1]. An analysis of the effect of speed on the generator load will be presented in this section.
The switch actuation angles are what determine the VRG operating mode. For this work, they were defined based on the tests of [1]. An analysis of the effect of varying these angles will be performed.
All the following analyses were performed on simulations performed with the computational platform presented in section 4, using the nonlinear model considering magnetic saturation demonstrated in section 3.

4.1. Ignition

The operation of the self-excited generator begins with the excitation cycle of the first activated phase. Since the capacitor has not yet been charged, the current for this cycle comes from the excitation source. Figure 13 shows the current coming from the source, the current in the capacitor and the current in the phase, and the firing angle.

It is possible to observe in Figure 13 that the source current is greater than the excitation current in phase A. This occurs because the current coming from the source is divided into 3, the first performs the initial charging of the capacitor, the second excites the phase and the third goes to the load, until the first switching occurs and the excited phase generates current.
The generated current is divided into two; the first goes to the capacitor and the second to the load. At this point, the diode is reverse-polarized, acting as an open circuit, and the excitation source no longer exerts influence on the circuit.

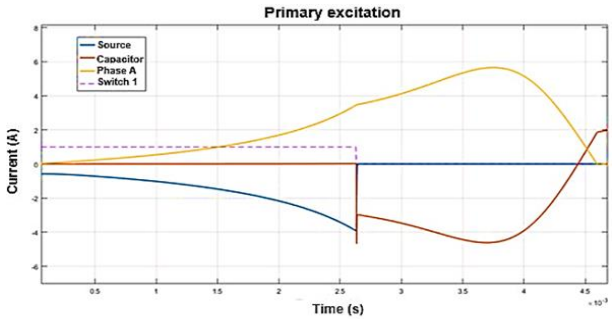

Fig. 13: Currents of the First Excitation Cycle.

From this point on, the capacitor starts to supply the excitation current to the phases. At each switching, it is recharged by the generating phase and discharged, exciting the next phase. This process can be seen in Figure 14.

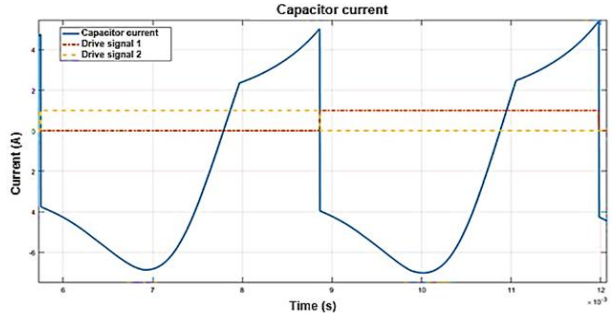

Fig. 14: Current in the Capacitor During Excitation.

The portion of the current in the capacitor with a negative value represents the moment in which the phase is generating current and recharging it. At the same time, the next phase is exciting. After the phase is completely demagnetized, the capacitor maintains the excitation until it reaches the magnetization peak, which is represented in the positive region of the curve. When the switching between the trigger signals occurs, the next phase generates current, and the effect is repeated. This phenomenon can be seen more clearly by comparing the current curve in the capacitor with the voltage induced in the phases. Figure 15 shows this comparison:

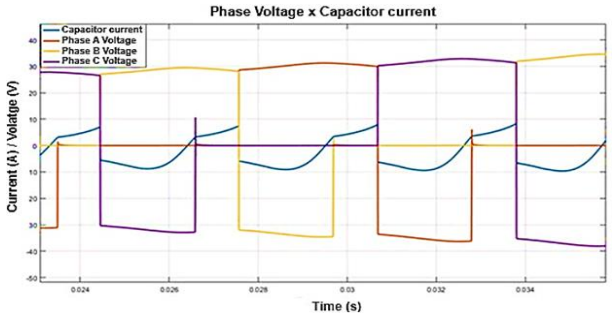

Fig. 15: Current in the Capacitor and Phase Voltages.

Current in the capacitor and voltages of phases A, B, and C. Source: Author's own. The portion of the voltage curves in the negative region refers to the voltage induced in the phase generation period, the moment when the capacitor is charged. The voltage curve of a phase is reduced to zero when it is completely demagnetized. At the same time, the next phase is exciting. Increases in the excitation voltage and current levels are noted during ignition. These increases occur due to the positive feedback cycle:
The excitation current increases the concatenated flux, and the electromechanical conversion occurs, generating more current, further increasing the flux. Part of the generated current is stored by the capacitor and made available during the excitation of the next phase. In this way, the excitation current of the new permutation is greater than the previous one, further increasing the flux. As a consequence, a higher voltage is induced in the next phase, since according to Ohm's law, voltage and current are directly proportional.
The cycle repeats until the magnetic saturation of the material occurs, reaching stability and entering a steady state. When magnetic saturation occurs, the concatenated flux does not increase beyond its limit; therefore, it does not increase the current, and this moment marks the end of the transient period. The VRG starts to generate enough current to excite itself and supply the load. Thus, the generated current presents two patterns of behavior, the incremental during the ignition and the saturated one in steady state. Figure 16 shows the phase and capacitor currents during the transient and steady state.

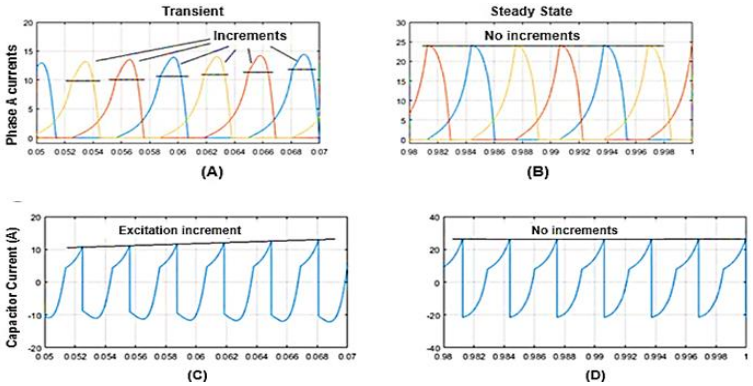

Fig. 16: Phase and Capacitor Currents (A) Phase Currents in the Transient Regime; (B) Phase Currents in Steady State; (C) Capacitor Current in Transient Regime; (D) Capacitor Current in Steady State.

The peak recorded between the phase currents was 24.23A. In Figure 16(A), straight lines were drawn at the point where the activation signal changes. The portion of the current above these straight lines is the increments generated. The effect of these on the capacitor current can be seen. In Figure 16(C), it is possible to draw an increasing straight line connecting the excitation peaks. The effect of the increments decreases until it reaches the steady state. Figures 16(B and D) correspond to the phase currents and the capacitor in steady state. The straight lines drawn show that the system has reached stability and the increments have ceased.

4.2. Analysis of voltage and current response at varying speeds under constant load in self-excited VRG operation

The following simulations were performed with the computational platform presented in section 4, the VRG 6x4 in self-excited mode, with a discrete interval of 1e-05, the load was fixed at 40Ω, the excitation source at 20V, and the speeds changed for each simulation, the values were 800 rpm, 1200 rpm, 1600 rpm, and 2000 rpm. Figure 17 shows the load voltage for the defined speeds.

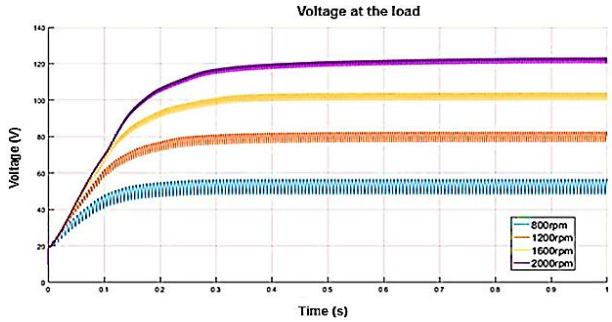

Fig. 17: Load Voltages for Varying Speeds.

Observing Figure 17, the increase in speed results in an increase in voltage. The average voltage values in steady state were 52.2 V for 800 rpm, 79.7 V for 1200 rpm, 102 V for 1600 rpm, and 122 V for 2000 rpm.
The increase in speed also reduces the oscillation of voltage levels in the load and changes the duration of the transient regime. These effects are also observed in the current curves in the load, illustrated in Figure 18.
The straight lines mark approximately the points where the current increases end, showing that the transient is prolonged with the increase in speed, just as the oscillations were reduced. The average values recorded for current in steady state were 1.29 A for 800 rpm, 1.98 A for 1200 rpm, 2.54 A for 1600 rpm, and 3.04 A for 2000 rpm.

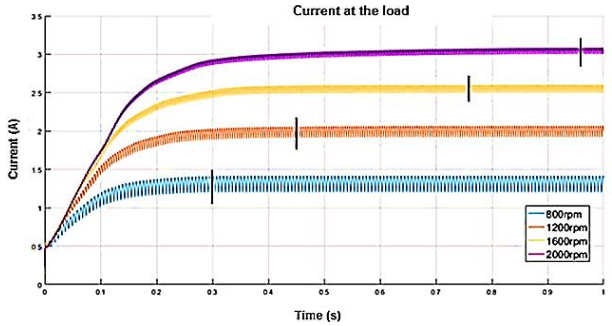

Fig. 18: Load Currents for Varying Speeds.

Figure 19 shows the current of a phase in transient and steady state, for each speed. The current peaks recorded were 24.38 A for 800 rpm, 25.54 A for 1200 rpm, 24.67 A for 1600 rpm, and 23.84 A for 2000 rpm.

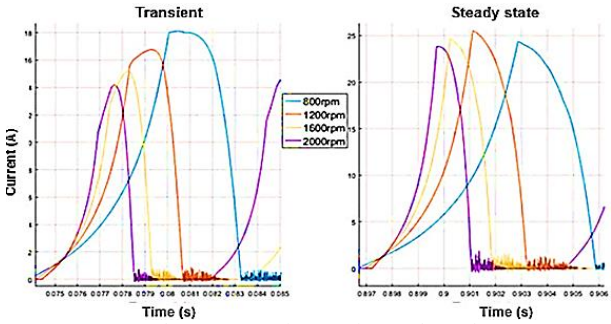

Fig. 19: Phase Currents in Transient and Steady State.

It is noted that the speed applied to the machine's rotor is inversely proportional to the period of activation of the switches, that is, the higher the rotation, the shorter the excitation time of the VRG phases.
Due to this factor, a longer excitation period accelerates the ignition. In Figure 19, it can be seen that in the same time interval, the current curve for 800 rpm has a higher peak value than the others. However, in a steady state, the peak currents are almost equal. Therefore, a higher frequency in generation makes a difference. Higher speeds deliver more voltage and current to the load.

4.3. Analysis of voltage and current behavior under varying load resistances and rotational speeds

The simulations performed previously were repeated with the same parameters and speeds. The load was changed between values of 10 Ω, 20 Ω, 40 Ω, and 80 Ω to observe the behavior of the generated voltage.
By observing Figures 20-24, it is possible to note that for all speeds, the increase in load resulted in an increase in voltage and a reduction in current.

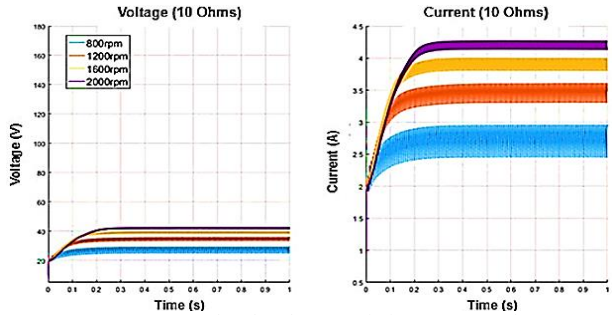

Fig. 20: Speed and Voltage Variation, 10 Ω Load.

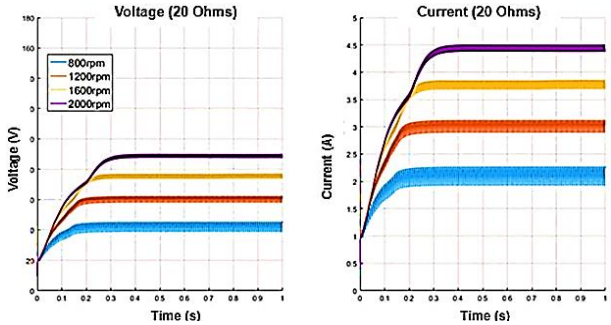

Fig. 21: Speed and Voltage Variation, 20 Ω Load.

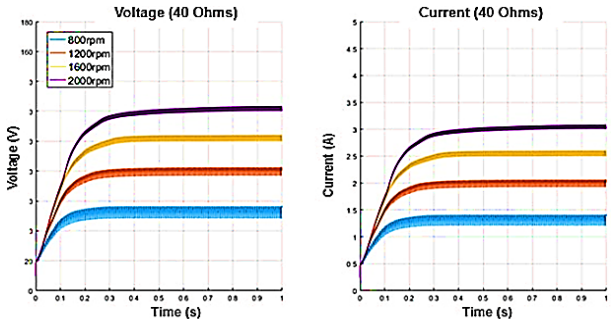

Fig. 22: Speed and Voltage Variation, 40 Ω Load.

Voltage and current in the 40 Ω load, each curve corresponds to a speed: 800 rpm in blue; 1200 rpm in red; 1600 rpm in yellow; 2000 rpm in purple.

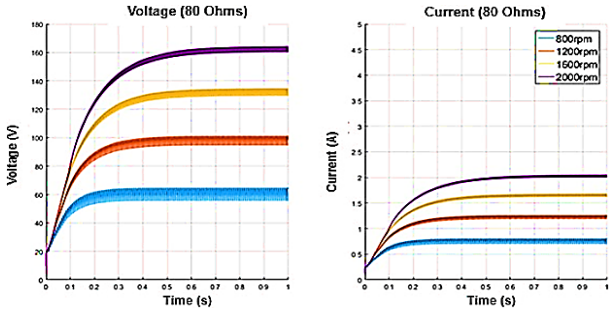

Fig. 23: Speed and Voltage Variation, 80 Ω Load.

Voltage and current at the 80 Ω load, each curve corresponds to a speed: 800 rpm in blue; 1200 rpm in red; 1600 rpm in yellow; 2000 rpm in purple.
The increase in speed has the same effect for all loads: reduction of oscillation in steady state, an increase in voltage and current at the load, and the transient regime is prolonged. Figure 24 shows the graphs of voltage at the load by speed, for all simulated loads.

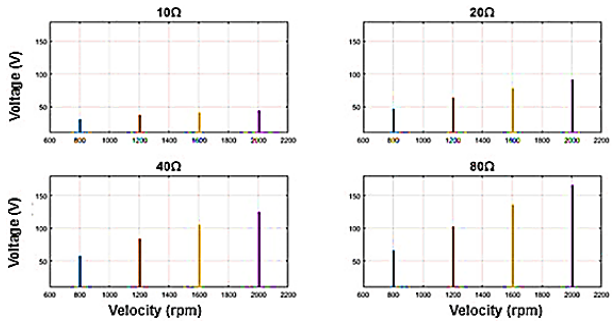

Fig. 24: Voltage by Speed.

For all simulated loads, the increase in speed resulted in an increase in voltage at the load, an almost linear relationship, as can be seen in the graphs in Figure 24. Increasing the speed from 800 rpm to 2000 rpm for a load of 10 Ω resulted in a 48.27% increase in the voltage value, while for the maximum load of 80 Ω, the increase was 145.58% for the same speed variation.

4.4. Change in actuation angles

The actuation angles of this work were defined based on tests previously performed by Bernadeli in [1]. To verify the proficiency of the angles, new simulations were performed, with a discrete time of 1e-05, fixed shaft speed of 2000 rpm, loads of 10 Ω, 20 Ω, 40 Ω, and 80 Ω, and the actuation angles were translated to the left and right.
It is worth mentioning that the actuation period is not changed when increasing or decreasing the on/off angles. For example, increasing +1° in the phase A actuation angles, on 85.3° and off 25.3° become on 86.3° and off 26.3°, the time interval in which the switches are actuated is the same, it will only be shifted to the right, that is, changing both angles with the same value the actuation is delayed or advanced. Figure 25 shows the voltage curves in the 10 Ω load, the angles changed between -4° and +4°, for transient and steady state.

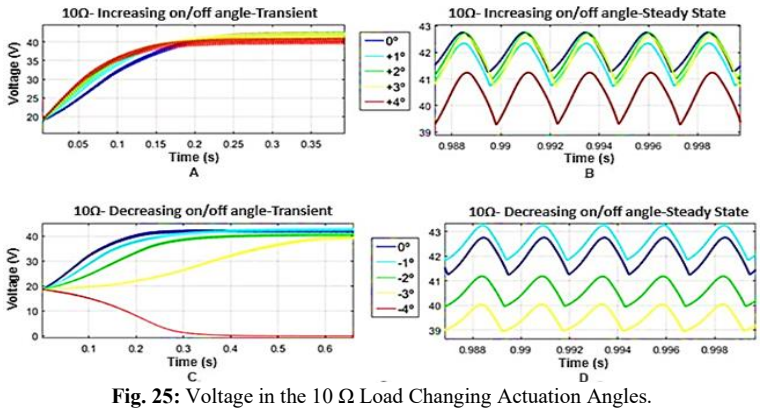

Fig. 25: Voltage in the 10 Ω Load Changing Actuation Angles.

Voltage in the 10 Ω load changing actuation angles: (A) Increase in the angle in transient regime; (B) Increase in the angle in steady state; (C) Reduction in the angle in transient regime; (D) Reduction in the angle in steady state.
For the 10 Ω load, the increase in the switch actuation angle causes an acceleration in the machine's transient period, as seen in Figure 25(A), but reduces the voltage in steady state in relation to the initial angle, as seen in Figure 25(B). Decreasing the angles increased the transient regime, as seen in Figure 25(C). The -4° angle resulted in an operating failure with the generator unable to self-excite, while -1° resulted in an increase in the voltage in steady state, as seen in Figure 25(D). Figure 26 shows the results for the simulation with a 20 Ω load.

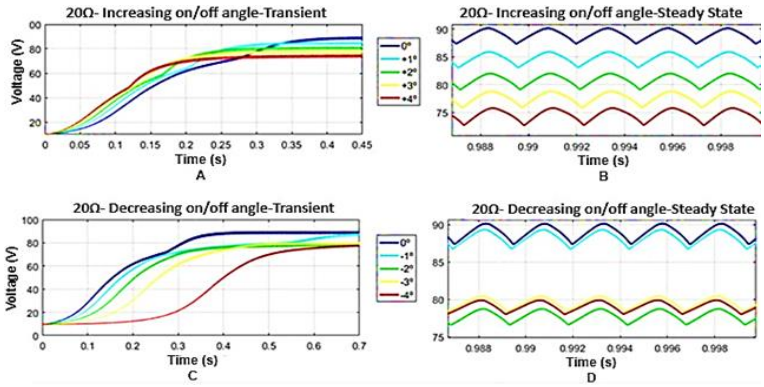

Fig. 26: Voltage at the 20 Ω Load Changing Actuation Angles.

Voltage at the 20 Ω load changing actuation angles: (A) Increase in the angle in transient regime; (B) Increase in the angle in steady state; (C) Reduction in the angle in transient regime; (D) Reduction in the angle in steady state.
For the 20 Ω load, the increase in the switch actuation angle has a similar effect to that of the 10 Ω load, as seen in figures 26 (A and B), accelerating the transient regime and reducing the voltage level in steady state. Decreasing the angles prolonged the transient regime, unlike the previous load, the last angle (-4º) managed to self-excite the machine, no angle increased the tension in steady state, as seen in figures 26 (C and D). Figure 27 refers to the simulations for the 40 Ω load.

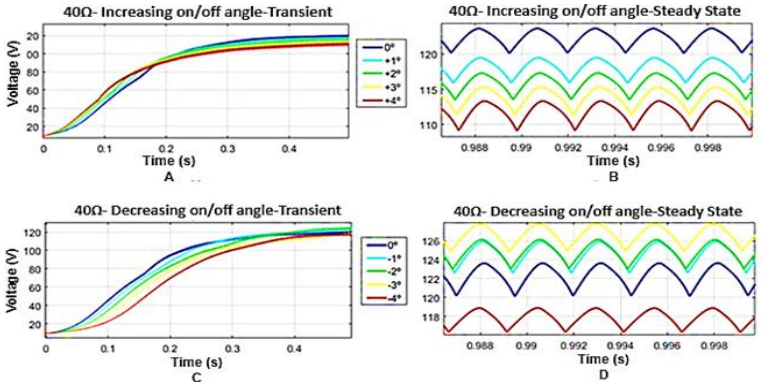

Fig. 27: Voltage in the 40 Ω Load Changing Actuation Angles.

Voltages in the 40 Ω load changing actuation angles: (A) Increase in the angle in transient regime; (B) Increase in the angle in steady state; (C) Reduction in the angle in transient regime; (D) Reduction in the angle in steady state.
For the 40Ω load, the increase in the switch actuation angle had the same effect as the previous loads, see figures 27(A and B). Decreasing the angles increased the transient regime, figure 27(C); however, the first 3 angles (-1º to -3º) increased the voltage in steady state, see figure 27(D).
Figure 28 shows the voltage curves for the 80Ω load. Increasing the switch actuation angle maintained the effect of the previous loads, figures 28(A and B). The decrease in angles increased the transient regime, Figure 28(C). For observation purposes, more simulations were carried out for this load. The angle was reduced until the voltage in steady state showed a drop from the previous angle. The first five angles (-1º to -5º) increased the voltage. From the sixth angle, -6°, the drop began, see figure 28 (D).

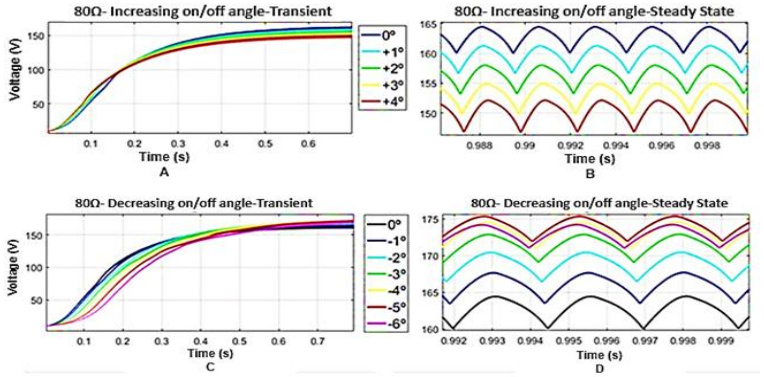

Fig. 28: Voltage at the 80 Ω Load Changing the Actuation Angles.

Voltage at the 80 Ω load changing the actuation angles: (A) Increase in the angle in the transient regime; (B) Increase in the angle in the steady state; (C) Reduction in the angle in the transient regime; (D) Reduction in the angle in the steady state.
The most expressive case among the simulations was the reduction of the angles by -5° for the 80 Ω load; for this reason, a comparison in relation to the reference (0°) is relevant. Figure 29 presents the current and power curves at the load, for 0° and -5.

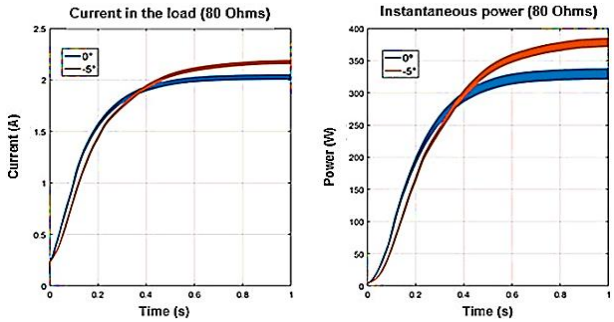

Fig. 29: Comparison of Current and Instantaneous Power.

With voltage and current higher than those of the reference angle, the simulation for advancing the on/off angles by 5° results in a higher instantaneous power delivered to the load. Figure 30 shows the comparison between the phase current in steady and transient conditions.

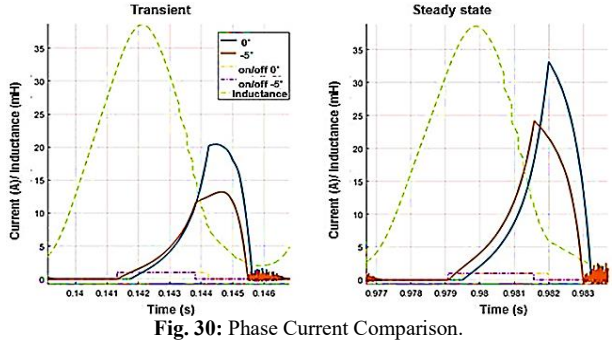

Fig. 30: Phase Current Comparison.

The reduction in the firing angle resulted in a decrease in the peak current from 33.19A to 24.21A. The simulation also revealed that the mechanical torque applied to the shaft was lower in relation to the reference, as can be seen in Figure 31.

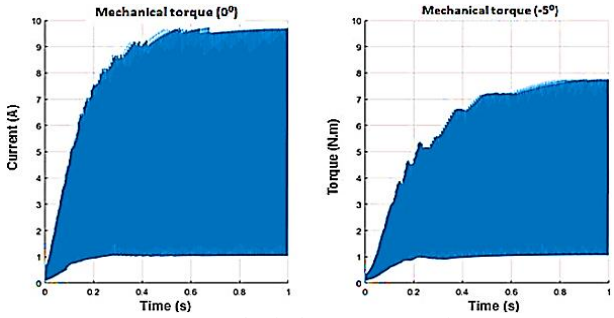

Fig. 31: Mechanical Torque Comparison.

These analyses do not detract from the optimal angles defined for the initial simulation, but demonstrate the importance of implementing an efficient control system, since, in this last analysis, the change in angles resulted in an increase in power delivered to the load, using less mechanical effort and with lower peak currents in the phases, which reduces the risks of the system, increasing its useful life.

This section presented an analysis of the transient regime of the self-excited VRG, called igniting. The positive feedback cycle responsible for the increases in voltage and current until reaching the steady state was discussed, with observations regarding the phase and capacitor currents.

The analysis of the effect of different speeds on the same load showed a behavioral pattern that was repeated for different loads: increasing the speed prolongs the transient regime, raises the voltage value in the load in steady state, and reduces oscillation.

Changing the drive angles presented adverse results for the different loads; the common point was their effect on the ignition; moving the drive to the right accelerates the transient regime, and to the left prolongs it.

Advancing the on/off angles by five degrees for the 80 Ω load with a fixed speed of 2000 rpm resulted in an improvement in the efficiency of the system, greater power delivered, lower torque used, and a lower peak current in the phases. This last analysis denotes the importance of implementing an efficient control system, a conclusion that is supported by the number of publications that contain or aim to control techniques for variable reluctance machines [1], [2], [6 - 9],[11], [12], [14 - 16].

4.5. Pilot study and empirical validation

To validate the simulation results and address the limitations inherent in pure computational analysis, a pilot experiment using the VRG 6x4 self-excited mode setup was performed at a lab scale. The hardware configuration included a 20V DC excitation source, an adjustable resistance bank between 10Ω and 80Ω, and a rotational speed simulator for test speeds of 800, 1200, 1600, and 2000rpm. Velocity and torque measurements were performed using a digital oscilloscope and torque sensors with a sampling interval of 10μs and simulated discrete gauges (1e-05).

The empirical results show consistent trends with the simulation behavior—that is, an increase in speed leads to an increase in the load angle and a decrease in the steady-state oscillations. For example, at 2000rpm with a 40Ω load, the measured voltage is 118V, which is

very close compared to 122V. Similarly, the observed transient acceleration increases, and the load time varies with different resistance levels.

But there are differences. At lower speeds (e.g., 800 rpm), the real system exhibited slightly more subtle oscillations, probably due to uncorrected effects such as hysteresis, temperature effects on rod resistance, and switching time. In addition, noise and electromagnetic interference affect signal purity during fast transmission.

To further investigate the control response, limited angular offset tests were also performed manually by advancing and delaying the switching signal with a microcontroller timer. These physical experiments confirmed the simulation conclusions that angle development decreased the peak torque of the wave, such that the efficiency gain-time peak values were higher by 5–10% due to conversion losses and sensor errors.

Overall, this preliminary validation supports the reliability of the simulation framework and strengthens the practical significance of the angular structure and velocity–load relationships. It also implies the need for closed-loop control, especially to compensate for physical nonlinearities that are difficult to capture in idealized simulation models. Future work will implement real-time monitoring strategies and expand the experimental platform to include inductive and dynamic loads.

4.6. Comparing open-loop results with closed-loop strategies

The open-loop simulations presented in this study provide valuable insights into the power behavior of a variable speed generator (SRG) at different speeds, load resistances, and operating angles. However, the results also show some limitations, notably the lack of active monitoring of the power and output power at different operating angles and transient time variations. These limitations are consistent with the motivations for developing management strategies explored in the literature.

For example, Touati et al. [9] modified the power control loop to improve stability, thereby improving the output curve and optimizing power generation—issues that remain with the open-loop strategy used in this paper. Similarly, Chirapo et al. [11] achieved precise power control with fast dynamic response and higher steady-state accuracy, exceeding the unsupervised response observed in earlier open-loop experiments.

Lee et al. [10] and Zahn et al. [13] focused on generator architectures and improved control methods (e.g., PT control), which have been shown to provide better power stability at different speeds and loads. These findings are inconsistent with the intensity fluctuations observed in our simulations and the long transients observed at low speeds and low loads.

Studies by Dos Santos Barros et al. [14] and Lu et al. [15] have shown that when applied to wind energy systems, power conversion efficiency can not only improve the operating speed of SRGs, but also demonstrate intelligent control capabilities to maintain high dynamic conditions.

Araujo et al. [16] further demonstrated that optimizing the switching angles using tracking and control techniques can improve efficiency, reduce mechanical torque requirements, and achieve lower phase current peaks - results similar to our findings 80]. 5). However, unlike closed-loop systems, such performance improvements in open-loop mode require precise regulation and cannot be adjusted in real time.

In summary, the open-loop approach allows the analysis of the basic behavior of the SRG, while the comparative study shows that the closed-loop strategy has advantages in improving power stability, reducing transients, increasing power output, and extending system lifetime. These results support the conclusion that the implementation of an efficient integrated control system is essential for the application of VRG/SRG systems.

Table 1: Summary of Efficiency and Voltage Metrics Across Operating Conditions

Speed (rpm)	Load (Ω)	Simulated Voltage (V)	Measured Voltage (V)	Simulated Current (A)	Measured Current (A)	Estimated Efficiency (%)
800	10	35.2	33.8	3.52	3.45	61.8
800	40	52.2	50.1	1.29	1.24	68.0
1200	40	79.7	76.9	1.98	1.92	72.3
1600	40	102.0	98.7	2.54	2.47	75.6
2000	40	122.0	118.0	3.04	2.96	78.4
2000	80	152.4	145.0	1.91	1.82	81.7
2000	80 (-5°)	162.7	155.8	2.03	1.94	85.2

The results in Table 1 show that there is a clear correlation between the increase in rotor speed and the improvement in power output and transition time under different load conditions, thereby improving the overall efficiency of the VRG system. For a fixed load of 40Ω, the voltage increases from 52.2V at 800rpm to 122V at 2000rpm, and the measured values also follow this trend. The deviation between the simulation results and the experimental results remains within a reasonable range (less than 7%), which can be attributed to practical losses such as switching efficiency losses, temperature effects, and power limitations, which are not considered in the simulation. The efficiency also increases with the increase in speed, from 68.0% to 78.4% under the same conditions, which is mainly due to better energy conversion and reduced oscillation behavior at higher frequencies. It is worth noting that lower loads (such as 80Ω) can further improve the efficiency to 81.7%, which may be due to the reduction in conduction losses and more stable power output.

The performance improvement is most significant when the operating angle increases by −5°, especially at 2000rpm and 80Ω. This adjustment results in a higher output voltage (simulated value of 162.7 V), higher output power, and lower peak current and mechanical torque, with a final efficiency of 85.2%. These results confirm the simulation results that adjusting the firing angle significantly affects the performance, especially in the absence of a feedback mechanism. However, the inability of the open-loop system to adapt in real time limits its ability to cope with changing operating conditions.

Comparing these observations with the strategies reported in the literature, a commonality emerges: active control significantly improves the robustness and efficiency of the system. For example, studies by Touati et al. [9] and Chirapo et al. [11] show that power control loops can reduce power losses and improve power quality. Similarly, studies using improved control algorithms or real-time optimization (e.g., Zan et al. [13], Araujo et al. [16]) have shown better dynamic adaptability of the switching angle and firing time at different speeds and loads. Therefore, this transparent analysis provides a solid foundation for understanding the behavior of VRGs, which in turn emphasizes the importance of implementing inter-beam control systems to bridge the gap between simulation and reality and improve performance in real applications.

5. Conclusions

This work explains the operating principles of the VRM, based on the tendency of the rotor to move in alignment with the position of least reluctance. The operation requires the activation of each phase in isolation, requiring appropriate converters and controls.
The review of recent publications portrays the evolution of studies on the machine in recent years, showing its potential and the space it has gained in the academic environment, mainly in renewable energy and automotive applications.
It was found that it is impossible to perform simulations of the VRG in self-excited mode using linear models. If the nonlinearities of the machine are disregarded, the simulation presents results that do not match reality. The nonlinear model used considers the saturation of the machine's magnetic circuit, and the inductance profile was represented using the Fourier series, since it has a symmetrical and periodic shape. Using the model, it was possible to perform static simulations to obtain the inductance, flux, and torque profiles.
The information from a pre-existing prototype, the model, and the equations of state were implemented in the simulation computational platform, and the simulation environment was MATLAB/SIMULINK. The excitation strategy was the use of a capacitor in parallel, the chosen converter was the HB¸, and the simulations were performed in open loop.
The simulation platform allowed the analysis of the dynamic behavior of the VRG in self-excited mode; observations on the igniting, variable speed, and changes in the actuation angle were made.
It was observed that the increase in speed for all loads increased the transient regime, an increase in voltage at the load, and a reduction in the generated voltage oscillation.
The translation of the on/off actuation angles presents different results for different loads. Delaying the angles accelerates the ignition; however, it reduces the voltage in steady state for all loads. Advancing the angles prolonged the ignition and, in some loads, presented an improvement in the efficiency of the system.

References

[1] Gao, S., Wang, Q., Li, G., Qian, Z., Zhou, S., & Li, Z. (2021). A deflectable switched reluctance motor/generator for wave energy conversion and underwater propulsion systems. *Journal of Electrical Engineering & Technology, 16*, 3157–3167. https://doi.org/10.1007/s42835-021-00773-x.

[2] Valdivia, V., Todd, R., Bryan, F. J., Barrado, A., Lazaro, A., & Forsyth, A. J. (2014). Behavioral modeling of a switched reluctance generator for aircraft power systems. *IEEE Transactions on Industrial Electronics, 61*, 2690–2699. https://doi.org/10.1109/TIE.2013.2267696.

[3] Zhu, Y., Wu, H., & Zhang, J. (2020). Regenerative braking control strategy for electric vehicles based on optimization of switched reluctance generator drive system. *IEEE Access, 8*, 76671–76682. https://doi.org/10.1109/ACCESS.2020.2990349.

[4] Diao, K., Sun, X., Lei, G., Guo, Y., & Zhu, J. (2021). Multimode optimization of switched reluctance machines in hybrid electric vehicles. *IEEE Transactions on Energy Conversion, 36*, 2217–2226. https://doi.org/10.1109/TEC.2020.3046721.

[5] Sun, X., Diao, K., & Yang, Z. (2019). Performance improvement of a switched reluctance machine with segmental rotors for hybrid electric vehicles. *Computers & Electrical Engineering, 77*, 244–259. https://doi.org/10.1016/j.compeleceng.2019.05.006.

[6] Bahy, M., Nada, A. S., Elbanna, S. H., & Shanab, M. A. M. (2020). Voltage control of switched reluctance generator using grasshopper optimization algorithm. *International Journal of Power Electronics and Drive Systems, 11*, 75. https://doi.org/10.11591/ijpeds.v11.i1.pp75-85.

[7] Chen, H., Xu, D., & Deng, X. (2021). Control for power converter of small-scale switched reluctance wind power generator. *IEEE Transactions on Industrial Electronics, 68*, 3148–3158. https://doi.org/10.1109/TIE.2020.2978689.

[8] De Oliveira, A. L., Capovilla, C. E., Santana Casella, I. R., Azcue-Puma, J. L., & Sguarezi Filho, A. J. (2021). Co-simulation of an SRG wind turbine control and GPRS/EGPRS wireless standards in smart grids. *IEEE/CAA Journal of Automatica Sinica, 8*, 656–663. https://doi.org/10.1109/JAS.2021.1003883.

[9] Touati, Z., Pereira, M., Araújo, R. E., & Khedher, A. (2022). Improvement of steady state performance of voltage control in switched reluctance generator: Experimental validation. *Machines, 10*, 103. https://doi.org/10.3390/machines10020103.

[10] Li, Z., Yu, X., Qian, Z., Wang, X., Xiao, Y., & Sun, H. (2020). Generation characteristics analysis of deflection type double stator switched reluctance generator. *IEEE Access, 8*, 196175–196186. https://doi.org/10.1109/ACCESS.2020.3034467.

[11] Chirapo, K. A. C., Oliveira, A. L., Sguarezi Filho, A. J., Pelizari, A., Di Santo, S. G., & Costa, E. C. M. (2020). P+RES controller applied to the direct power control of switched reluctance generator. *Journal of Control, Automation and Electrical Systems, 31*, 360–366. https://doi.org/10.1007/s40313-019-00543-1.

[12] Sarr, A., Bahri, I., Berthelot, E., Kebe, A., & Diallo, D. (2020). Switched reluctance generator for low voltage DC microgrid operation: Experimental validation. *Energies, 13*, 3032. https://doi.org/10.3390/en13123032.

[13] Zan, X., Ni, K., Zhang, W., Jiang, Z., Cui, M., Yu, D., & Zeng, R. A. (2019). New control strategy for SR generation system based on modified PT control. *IEEE Access, 7*, 179720–179733. https://doi.org/10.1109/ACCESS.2019.2959088.

[14] dos Santos Barros, T. A., dos Santos Neto, P. J., Nascimento Filho, P. S., Moreira, A. B., & Ruppert Filho, E. (2017). An approach for switched reluctance generator in a wind generation system with a wide range of operation speed. *IEEE Transactions on Power Electronics, 32*, 8277–8292. https://doi.org/10.1109/TPEL.2017.2697822.

[15] Lu, M. Z., Jhou, P. H., & Liaw, C. M. (2021). Wind switched-reluctance generator based microgrid with integrated plug-in energy support mechanism. *IEEE Transactions on Power Electronics, 36*, 5496–5511. https://doi.org/10.1109/TPEL.2020.3029528.

[16] Araujo, W. R. H., Reis, M. R. C., Wainer, G. A., & Calixto, W. P. (2021). Efficiency enhancement of switched reluctance generator employing optimized control associated with tracking technique. *Energies, 14*, 8388. https://doi.org/10.3390/en14248388.